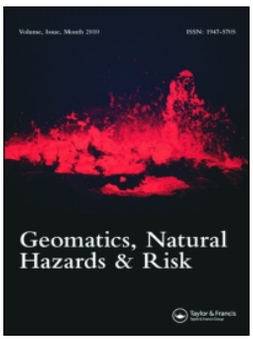

Geomatics, Natural Hazards and Risk

ISSN: 1947-5705 (Print) 1947-5713 (Online) Journal homepage: https://www.tandfonline.com/loi/tgnh20

Monitoring the deformation of a concrete dam: a case study on the Deriner Dam, Artvin, Turkey

Berkant Konakoglu, Leyla Cakir & Volkan Yilmaz

To cite this article: Berkant Konakoglu, Leyla Cakir & Volkan Yilmaz (2020) Monitoring the deformation of a concrete dam: a case study on the Deriner Dam, Artvin, Turkey, Geomatics, Natural Hazards and Risk, 11:1, 160-177, DOI: 10.1080/19475705.2020.1714755

To link to this article: https://doi.org/10.1080/19475705.2020.1714755

© 2020 The Author(s). Published by Informa UK Limited, trading as Taylor & Francis Group

Published online: 28 Jan 2020.

Submit your article to this journal

Article views: 66

View related articles

View Crossmark data

Full Terms & Conditions of access and use can be found at
https://www.tandfonline.com/action/journalInformation?journalCode=tgnh20

GEOMATICS, NATURAL HAZARDS AND RISK
2020, VOL. 11, NO. 1, 160–177
https://doi.org/10.1080/19475705.2020.1714755

Taylor & Francis
Taylor & Francis Group

OPEN ACCESS Check for updates

Monitoring the deformation of a concrete dam: a case study on the Deriner Dam, Artvin, Turkey

Berkant Konakoglu[a], Leyla Cakir[a] and Volkan Yilmaz[b]

[a]Department of Geomatics Engineering, Karadeniz Technical University, Trabzon, Turkey;
[b]Department of Geomatics Engineering, Artvin Coruh University, Artvin, Turkey

ABSTRACT

This paper investigates the behaviour of the double-curvature Deriner dam, which is in the operation phase and also one of the highest dams in the world. In order to determine the displacements, a geodetic network consisting of twelve reference and seven object points was measured in four periods by means of the Global Navigation Satellite Systems (GNSS) data. The θ^2-Criteria method was used to determine the extent of the deformation. The deformation analysis results based on the GNSS measurements revealed significant horizontal and vertical displacements on the object points on the dam crest. Hence, the vertical displacements found based on the GNSS measurements can be considered erroneous, because they are greater than expected. This may be due to the narrow topography of the valley. Another conclusion drawn from the results is that there is a strong relationship between the change in the reservoir water level and horizontal deformations, as can be seen from the horizontal deformation vectors.

ARTICLE HISTORY
Received 11 November 2019
Accepted 4 January 2020

KEYWORDS
Geodetic monitoring; deformation analysis; GNSS; Deriner Dam

1. Introduction

In the last two decades, more than 200 hydroelectric power plants have been established in the Black Sea Region of Turkey (Kanik and Ersoy 2019). The Coruh River basin, which is the longest river in the East Black Sea Region, has a huge potential to construct dams thanks to the favourable topographical conditions of the region. There are several dam projects on Coruh river basin, some of which are under construction and some are in already operation phase. Of these, the Deriner (Lower Coruh), a super-high-arch dam, is one of the most important projects of the master plan of Coruh River basin. Monitoring the dams with such high construction costs is crucial for their safety and starts during the construction phase and maintains during its lifespan. There are different factors that could cause the destruction of the arch dams, including its self-weight, hydrostatic pressure on the upstream surface, internal

CONTACT Berkant Konakoglu berkantkonakoglu@gmail.com

© 2020 The Author(s). Published by Informa UK Limited, trading as Taylor & Francis Group.
This is an Open Access article distributed under the terms of the Creative Commons Attribution License (http://creativecommons.org/licenses/by/4.0/), which permits unrestricted use, distribution, and reproduction in any medium, provided the original work is properly cited.

temperature changes etc. Over the years, several studies have been conducted to monitor the behaviour of dams (Tarchi et al. 1999; Manake and Kulkarni 2002; Pytharouli and Stiros 2005; De Sortis and Paoliani 2007; Mascolo et al. 2014; Talich 2016; Saidi et al. 2017; Di Pasquale et al. 2018; Xi et al. 2018; Yavaşoğlu et al. 2018; Xiao et al. 2019). For example, Guler et al. (2006) investigated the horizontal and vertical surface movements on the Alibey Dam using geodetic and non-geodetic techniques. The geodetic measurements were conducted on a micro-geodetic network consisting of 10 reference and 16 object points between the years of 1987–1991 and 1991–1996. These measurements were analysed using the Karlsruhe method. Also, the Finite Element Method (FEM) was used to determine the behaviour of the dam under two-dimensional plane-strain conditions. The results of numerical analyses were compared against those of the geodetic analysis. The authors concluded that almost the same results were obtained by these two analysis techniques in terms of magnitude. Kulkarni et al. (2006) proved that it was possible to use the GPS on the Koyna Dam to calculate the movements occurred as a result of the earthquakes. An extensive GPS network with 31 points was established and more than ten GPS campaigns were conducted between December 2000 and September 2004. The results demonstrated a correlation between the water level and movements. Bayrak (2008) investigated the relationship between the reservoir water level and displacement on the dam. Fifteen points consisting of 6 reference and 9 object points were observed within 4 periods (December 2003, March 2004, November 2004 and April 2005) using a total station. A new dynamic deformation analysis approach was developed to investigate how the changing reservoir water level affected the vertical and horizontal displacements during the first filling phase. The results derived from the dynamic model revealed that the change in the reservoir water level is an important factor for Yamula Dam deformations. Gikas and Sakellariou (2008) analysed the long-term (about thirty years) settlement behaviour of the Mornos Dam. Precise leveling observations and a numerical back analysis model data sources were used to determine the vertical displacements at the dam body. It is crucial to acknowledge that 60% of these displacements originated during the construction and first filling phase, as the remaining 40% occurred during the operation phase. According to the results, the maximum displacement was observed at the middle of the dam crest. In addition, an average of 0.03 m agreement was found between the results obtained based on the numerical back analysis and the results based on the geodetic measurements. Ehiorobo and Ehigiator (2011) investigated the use of differential GPS (DGPS) to monitor the horizontal displacements at the Ikpoba dam (Earth). Along the dam crest, 20 GPS points including 11 reference and 9 object points were observed within three period measurements conducted between 2008 and 2010. It was concluded that all object points moved in the south-west direction, which may be due to the hydrostatic pressure. Taşçı (2008) utilized four-period Global Positioning System (GPS) data to monitor the horizontal movements on the Altınkaya Dam. A deformation network, which consisted of 6 reference and 11 object points, was established to monitor horizontal movements. The Iterative Weighted Similarity Transformation (IWST) and Least Absolute Sum (LAS) methods were used to decide whether or not the points were stable. The results showed that the largest movements were at the

middle and at the end points of the dam crest. Kalkan (2014) investigated the magnitude and direction of radial deformations on the rock-fill Ataturk dam, which was constructed on the Firat (Euphrates) River. The deformations at the Ataturk dam were investigated by utilizing the GPS and conventional measurement data, which were collected between 2006 and 2010. According to the results, the largest deformations were found on the upstream part of the crest. It was also concluded that the results obtained from the GPS and conventional measurement data had a comparable accuracy ($< \pm 1$ cm). Besides, the study examined if there was a relationship between the reservoir water level and deformation at the points on the dam. No significant relationship was found between the radial displacements and reservoir water level. Yigit et al., (2016) investigated the horizontal displacements during the first filling of the Ermenek dam, which is a double-curvature asymmetrical thin concrete arch dam located at Karaman Province, Turkey. The displacements were determined through a network with 10 reference and 19 object points. The authors used nine-period geodetic measurements conducted between 2011 and 2012 with total station and prisms. The FEM was used to calculate possible radial displacements. The results showed that there was a high correlation between the geodetic and numerical methods with regard to displacement values. Also, an approximate increase of 58 m in water level during the first filling phase was found to cause 1 cm displacement in the dam body. Acosta et al., (2018) examined the behaviour of the Arenoso Earth Dam through the use of high-precision leveling and Global Navigation Satellite System (GNSS) techniques. They determined the displacements by the FEM. Seven GNSS campaigns were conducted between February 2008 and September 2016. A comparative evaluation of the results derived from the geodetic techniques and FEM indicated that there were an average of 6 cm and 20 cm differences between the horizontal and vertical displacements at the dam crest, respectively. These differences were probably due to the simplification assumed during the application of the FEM. Barzaghi et al. (2018) examined the movements at the Cantoniera Dam (Eleonora D'Arborea), built for drinking water, irrigation and hydroelectric energy production, using three different instruments, which were GNSS, collimators and pendulums. However, only the GNSS and pendulums data were compared and collimator data were evaluated separately. The Leica GNSS spider software was used to process the GNSS data. Despite the fact that the GNSS was less sensitive than a pendulum, it was observed that only the GNSS technique was adequate for precise monitoring of the dam.

This study aims to investigate the horizontal and vertical displacements on the Deriner Dam between 2016 and 2017. To achieve this, the GNSS and high-precision leveling measurements were conducted within four periods. Since the high precision leveling measurements were not accurate enough to determine the vertical displacements due to windy weather during periods, the results for these measurements were not given in this paper. In addition, we tried to find out whether any changes in the water level of the reservoir affected the horizontal and vertical displacements of the dam during the operation phase.

The rest of the paper is organised as follows. Section 2 provides background information about the deformation method using the GNSS measurements. Section 3 introduces the Deriner Dam and geodetic networks used. Section 4 presents the

results based on the GNSS measurements. Finally, some concluding remarks are given in Section 5.

2. Deformation analysis with θ^2-criteria method

Many researchers have attempted to determine any displacements utilizing θ^2-criteria method in many deformation-related applications such as bridge (Erol et al. 2005), mining (Kayikci and Yalcinkaya 2015), earthquake (Ozener et al. 2013; Sabuncu and Ozener 2014; Tiryakioglu et al. 2019), landslide (Yalçinkaya and Bayrak 2005; Acar et al. 2008; Hastaoğlu 2013; Zeybek et al. 2015), dam (Bayrak 2007). In order to detect any displacements with θ^2-criteria method, the geodetic network is measured at least two different observation times with geodetic methods. The displacements of points are tested with statistical methods. These tests are conducted for the data of two observation periods using the Gauss-Markov model. The Gauss-Markov model for a geodetic network is given as follows (Caspary 1988):

$$\begin{aligned} l + v &= Ax \\ x &= (A^T PA)^+ A^T Pl, \;\; Q_{xx} = (A^T PA)^+ \\ Q_{vv} &= P^{-1} - AQ_{xx}A^T \\ s^2 &= \frac{v^T Pv}{f} \end{aligned} \tag{1}$$

where l is the observations vectors; v is the residuals vectors; A is the design matrix; x is the vector of estimated unknown parameters; Q_{xx} and Q_{vv} are the cofactor matrices of the unknowns and residual vectors, respectively; P is the weights matrix; s^2 is the posteriori variance of the unit weight; and f is the degree of freedom. Hypotheses are written to investigate whether there are any statistically significant movements between periods t_1 and t_2. H_0 and H_A hypothesis are formed as follows:

$$H_0 : E(d) = E(x_2) - E(x_1) = 0 \tag{2}$$

and

$$H_A : E(d) = E(x_2) - E(x_1) \neq 0 \tag{3}$$

where E stands for the 'expectation' and H_A denotes the alternative hypothesis. In the absence of correlation, the test statistics is given as follows (Pelzer 1971, 1985, Koch 1985, Niemeier 1985, Cooper 1987):

$$d = x_2 \; - \; x_1 \tag{4}$$

$$Q_{dd} = Q_{x_i x_i} + Q_{x_j x_j} \tag{5}$$

$$\theta^2 = \; d^T Q_{dd}^+ d \tag{6}$$

$$T = \frac{\theta^2}{s_0^2\ h} \sim F_{h,f,1-a} \tag{7}$$

where d is the coordinate differences vector; Q_{dd} is the cofactor matrix of vector d; Q_{dd}^{+} is pseudo inverse; h is the rank of the matrix Q_{dd} and a is the chosen error probability. If $T > F_{h,\ f,1-a}$, then the H_0 hypothesis is rejected, and the point can be regarded as unstable. Otherwise, $T \leq F_{h,\ f,1-a}$, then the H_0 hypothesis is not rejected, and it can be stated that the point is not significantly displaced. After that, localization procedure is carried out. The coordinate differences vector d and Q_{dd}^{+} are decomposed into the subvectors and submatrices as follows:

$$d = \begin{bmatrix} d_r \\ d_j \end{bmatrix} \tag{8}$$

$$Q_{dd}^{+} = \begin{bmatrix} P_r & P_{rj} \\ P_{jr} & P_j \end{bmatrix} \tag{9}$$

where indexes r and j denote the stable and unstable points, respectively. θ^2-criteria are calculated for unstable points as follows:

$$\left(\theta_j^2\right)_i = \left(\overline{d}_j^{\,T} P_j\ \overline{d}_j\right)_i, i = 1, 2, \ldots, n \tag{10}$$

where $\overline{d}_j = d_j + \ P_j^{-1}\ P_{ji}\ d_r$ and n is the number of points. The point with the maximum θ_j^2 is considered unstable and removed from the current datum. The remaining points are used to define a new datum with the S-transformation method. The iteration is repeated until there are no unstable points among the remaining points. Thus, unstable points are detected. Further details regarding S-transformation can be found in Teunissen (1985).

3. Application

The Deriner dam is located at the downstream part of the Coruh River basin at Artvin province, in the north-eastern part of Turkey (see Figure 1). The Coruh River has an average flow rate of 154 m^3/s and the catchment area of the river is 18,390 km^2. The Deriner dam, a concrete double-curvature arch with a height of 249 m, has a crest length of 721 m. The underground powerhouse has a width of 20 m, a length of 126 m, and a height of 45 m, and includes four vertical Francis units with a total capacity of 670 MW. Two-gated spillway tunnels located at the right and left abutments and eight orifice spillways integrated onto the dam body are designed for flood discharge. Until 1 January 2019, a total of 8.7 billion kilowatt hours of energy was produced at the Deriner dam. Construction of the Deriner dam started in 1998, completed at the end of 2012 and became operational in mid-2013.

In order to determine any horizontal and vertical displacements by geodetic techniques, a geodetic network established by the General Directorate of State Hydraulic Works (DSI) was used. However, all reference points were not used in this study,

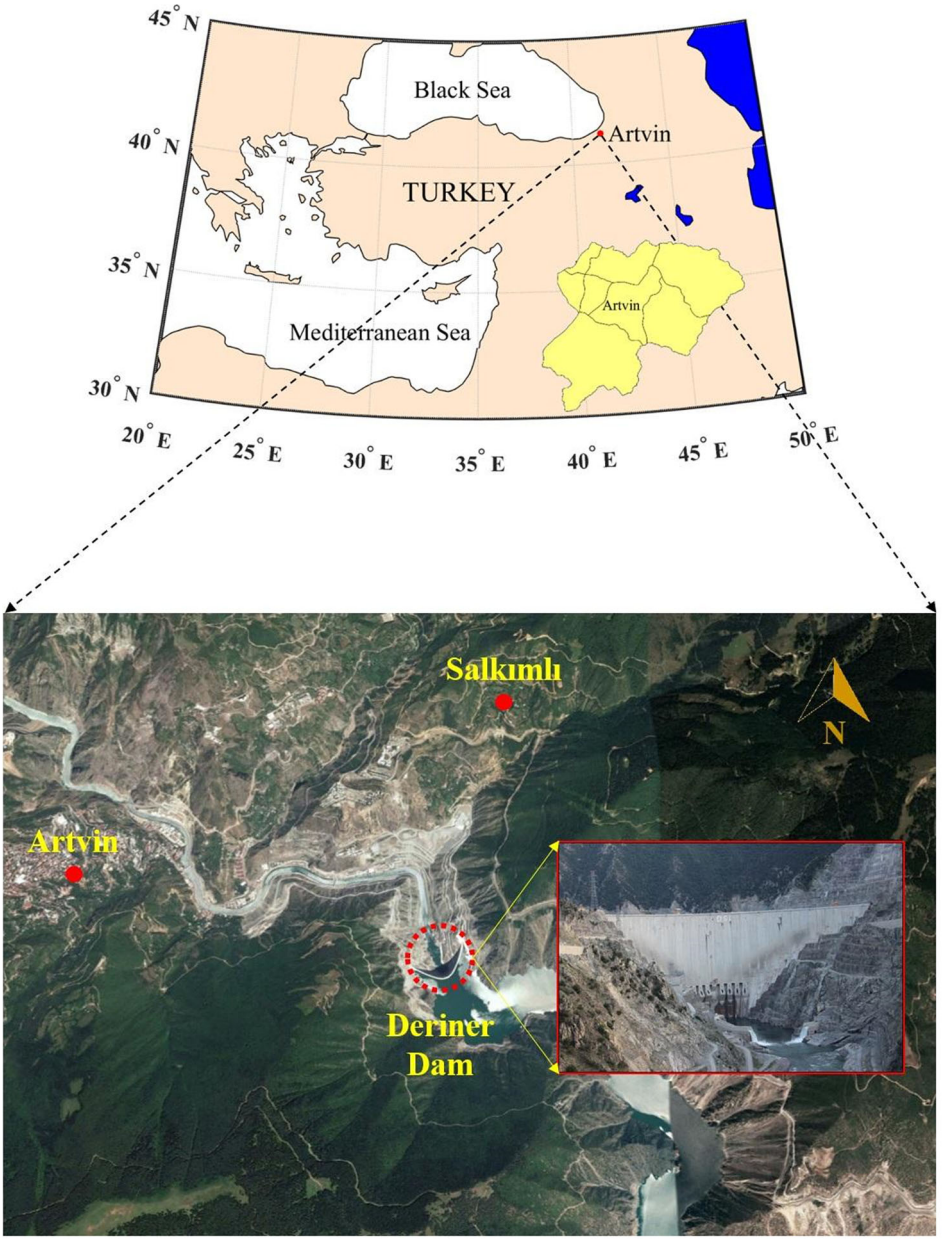

Figure 1. The Deriner Dam. Source: Author.

since some of them were deformed and some were too close to the dam crest to be measured by the GNSS. The network covered the whole study site and consisted of twelve reference points (101, 102, 104, 105, 107, 108, 109, 111, 112, 116, 117 and 118) and seven object points (1103, 1109, 1115, 1121, 1127, 1133 and 1139). All the points of the network were constructed as pillars which are double-walled concrete pipes to avoid alteration by sun radiations and temperature variations, and the forced centering system is used on these points to eliminate the centering errors. The reference

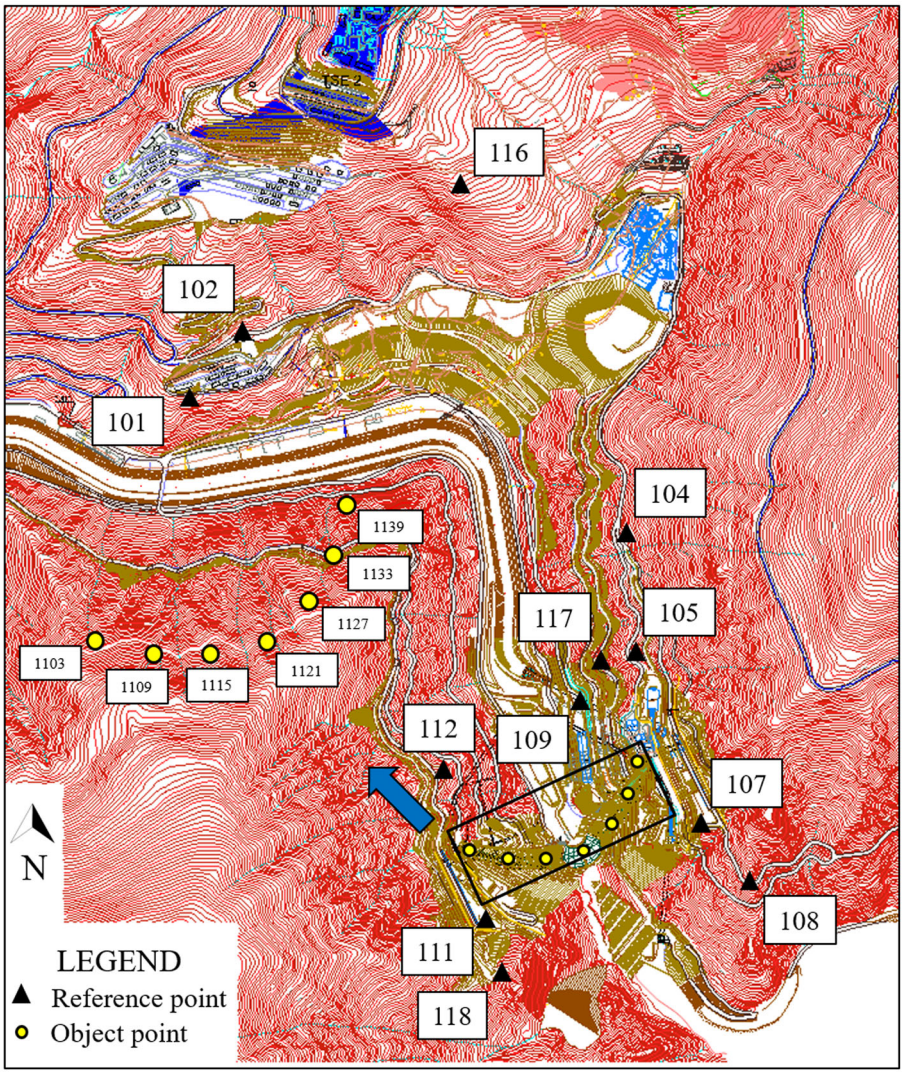

Figure 2. Distribution of the reference and object points. Source: Author.

points were established on geologically stable grounds, where the deformation was not expected. The reference points extended 300 m in upstream direction, 2 km in downstream direction and 800 m from the left to the right abutment of the Deriner dam. The object points were located on balconies of the dam crest and downstream side of the dam. Figure 2 shows the distribution of the reference and object points used in this study.

The GNSS data were collected in the static survey mode, using four Topcon HiPer Pro and four Topcon GR5 dual-frequency receivers. In all campaigns, the same GNSS receivers were used at the same points. Figure 3 shows two of the reference pillars on which the GNSS receivers were installed.

The measurements were conducted between 2016 and 2017, covering about 1.5 years. The first period measurement was carried out in May 2016, the second in

Figure 3. GNSS receivers installed on the reference pillars 102 (left) and 109 (right). Source: Author.

November 2016, the third in May 2017 and the last one in August 2017. Observation duration was selected at least 2 hours and 1 hour for the reference and object points, respectively. The object points were measured using the leapfrog method. The data-sampling rate and satellite elevation cut-off angle were set to 10 sec and 15°, respectively. The determination of displacements in the geodetic networks and interpretation of the behavior of the displacements are also possible by monitoring the movement more sensitively. Therefore, the network to be installed or used should be optimal in terms of precision and robustness. Baarda (1968) categorized the reliability into two parts, "internal reliability" and "external reliability". While internal reliability provides information about the maximum undetectable error that would not be determined by the model hypothesis, external reliability refers to the coefficient of undetectable model error on the estimates of unknown parameters. Baarda (1968), Yalçınkaya and Teke (2006) and Küreç and Konak (2014) provided further details about the reliability. The internal and external reliability values were calculated and compared against the critical values of the reliability levels.

The commercial Magnet Tools 5.1 software developed by the Topcon Inc. was used to process the recorded GNSS data. The software automatically selects the processing frequency. Since the baseline length of the vector did not exceed 10 km, it automatically selected the L1/L2 mode for processing static vectors. The broadcast ephemeris was used as the satellite orbit. The Magnet Tools 5.1 software is able to provide geocentric cartesian coordinates in the World Geodetic System 1984 (WGS84) datum. Since the geocentric cartesian coordinates cannot be used in structural health monitoring applications, they should be transformed into local topocentric coordinates (Yigit 2016). Hence, all geocentric cartesian coordinates and their cofactor matrices were transformed into a local topocentric coordinate system for

each period. The equations are given as follows:

$$\begin{bmatrix} e_i \\ n_i \\ u_i \end{bmatrix} = R(\Phi_0, \lambda_0) \begin{bmatrix} X_i - X_0 \\ Y_i - Y_0 \\ Z_i - Z_0 \end{bmatrix} \tag{11}$$

where φ_0 and λ_0 are the geodetic latitude and longitude of the topocentric origin, respectively. φ_0 and λ_0 are derived from their geocentric cartesian coordinates X_0, Y_0 and Z_0.

$$R(\Phi_0, \lambda_0) = \begin{bmatrix} -\sin(\lambda_0) & \cos(\lambda_0) & 0 \\ -\sin(\varphi_0)\cos(\lambda_0) & -\sin(\varphi_0)\sin(\lambda_0) & \cos(\varphi_0) \\ \cos(\varphi_0)\cos(\lambda_0) & \cos(\varphi_0)\sin(\lambda_0) & \sin(\varphi_0) \end{bmatrix} \tag{12}$$

Using the error propagation law, the cofactor matrix of each period in the local topocentric coordinate system is derived as follows:

$$Q_{e,n,u} = R(\Phi_0, \lambda_0)\ Q_{X,Y,Z}\ R(\Phi_0, \lambda_0)^T \tag{13}$$

where $Q_{X,Y,Z}$ is the cofactor matrix of the geodetic cartesian coordinate system. In this study, the point 1139 was selected as the origin of the topocentric coordinate system and the other points were reduced with respect to this point.

A MATLAB script was developed to adjust the geodetic network. The GNSS measurements were adjusted with respect to the free network adjustment method. Outlying observation(s) were detected using the Huber M-estimation method. This estimation provides the solution by reducing the weights of the suspicious observation(s) at each iteration. The reason for using this method was that it does not remove the outlying observation(s) from the measurement group. Further details about this method can be found in Huber (1981). In all processes, the significance level was chosen as $\alpha = 0.05$.

4. Results

The calculated redundancy values of the observations were compared against the selected critical value of 0.3. According to the results, none of the redundancy numbers exceeded the critical value. The internal and external reliability values of each baseline and their critical values were computed. The internal reliability values remained between 0.20 and 0.28 units, whereas the external reliability values remained between 0.08 and 0.11 units. The internal and external reliability values of the network were found under their critical values. According to the results of the reliability criteria, controllability rate of all the GNSS baselines could be qualified as "excellent".

The results of the reference and object points for the periods May 2016-November 2016, May 2016-May 2017 and May 2016-August 2017 are given in Tables 1–3, respectively. The object points of 1109, 1115, 1121, 1127, 1133 and 1139, which were on the dam crest, and the reference points of 101, 102, 104, 105, 108, 109, 112, 116, 117 and

Table 1. Results of the θ^2-criteria method between the periods May 2016 and November 2016.

Step	T	θ^2-criteria	Moving point	d_n(cm)	d_e (cm)	d_u (cm)	$d_{horizontal}$(cm)
1	213.98	995.82	112	−0.11	0.11	4.25	0.16
2	133.30	334.42	102	0.79	0.77	−3.37	1.10
3	126.50	380.52	1127	−1.04	1.07	−3.03	1.49
4	85.82	222.40	1121	−1.89	0.96	0.82	2.12
5	76.17	127.21	1109	−0.79	−0.43	−3.05	0.90
6	56.16	153.12	101	0.42	0.24	−3.46	0.48
7	35.77	78.19	1133	−0.64	0.92	−0.09	1.12
8	22.46	77.11	1115	−2.07	0.50	0.50	2.13
9	5.73	14.55	109	0.01	0.15	−0.46	0.15
10	5.46	9.92	108	−0.19	0.11	−0.36	0.22
11	5.52	9.22	1139	−0.13	0.03	−0.54	0.13
12	5.68	7.16	105	0.19	−0.04	−0.11	0.19
13	6.28	6.59	117	0.01	−0.02	−0.55	0.02
14	6.50	4.65	116	−0.19	0.53	0.01	0.56
15	2.51	2.55	118	−0.03	0.03	−0.45	0.04

Table 2. Results of θ^2-criteria method between the periods May 2016 and May 2017.

Step	T	θ^2-criteria	Moving point	d_n(cm)	d_e (cm)	d_u (cm)	$d_{horizontal}$ (cm)
1	173.86	1659.68	102	−2.00	2.04	−7.37	2.86
2	162.37	802.99	105	0.61	−0.30	4.87	0.68
3	102.36	376.97	101	0.57	0.18	−4.73	0.60
4	102.94	209.76	1121	−1.48	0.52	1.24	1.57
5	101.80	179.32	1115	−1.88	0.17	1.49	1.89
6	92.95	139.18	1127	−1.30	1.07	−2.40	1.68
7	65.90	116.10	1133	−0.96	0.95	0.66	1.35
8	61.73	99.93	112	0.04	−0.14	1.58	0.15
9	56.69	90.98	116	−0.02	0.49	−4.11	0.49
10	39.89	64.59	1109	−1.25	−0.11	−2.50	1.25
11	6.86	39.06	108	−0.57	0.21	0.58	0.61
12	4.94	24.33	118	−0.07	0.03	0.42	0.08
13	5.72	18.15	1103	−0.63	0.07	0.72	0.63
14	4.94	12.33	1139	−0.68	−0.03	0.41	0.68
15	5.46	9.11	107	−0.24	0.04	0.94	0.24
16	6.70	9.36	109	−0.38	0.02	0.86	0.38
17	5.98	0.83	104	−0.32	−0.09	0.64	0.33

Table 3. Results of θ^2-criteria method between the periods May 2016 and August 2017.

Step	T	θ^2-criteria	Moving point	d_n (cm)	d_e (cm)	d_u (cm)	$d_{horizontal}$(cm)
1	113.21	1469.39	102	−2.38	2.10	−5.95	3.17
2	100.77	534.34	116	0.64	−0.41	−4.70	0.76
3	93.00	375.34	1127	−1.47	1.69	−2.40	2.24
4	76.08	327.24	1121	−2.24	1.26	1.25	2.57
5	69.31	151.55	1115	−2.65	0.37	1.34	2.97
6	53.50	154.07	1133	−0.95	1.29	0.58	1.60
7	46.85	86.60	1109	−1.33	−0.32	−2.70	1.37
8	35.36	59.05	101	−0.08	−0.13	−2.63	0.15
9	33.03	39.76	108	−0.42	0.61	−1.11	0.74
10	29.07	18.92	105	0.03	0.15	1.76	0.15
11	19.99	19.30	109	−0.01	0.20	1.10	0.20
12	14.71	11.40	112	0.19	0.13	1.37	0.23
13	12.63	6.72	107	−0.49	−0.07	−1.28	0.49
14	13.85	4.70	104	0.16	−0.04	−0.70	0.16
15	14.89	6.04	118	0.28	0.15	−0.96	0.32
16	3.11	1.68	1139	−0.32	0.03	0.32	0.32

118 were detected as unstable between the periods May 2016 and November 2016. The reservoir water level dropped from about 389 m to 377 m between these periods.

The object point of 1103 and reference points of 104 and 107 were also detected as unstable between the periods May 2016 and May 2017, which leads to the fact that all object points on the dam crest moved. The reference point of 117 was regarded as stable during this period. In May 2017, the reservoir water level continued to decrease and reached 364 m.

As can be seen from Table 3, the reference points of 107 and 117, and the object point of 1103 were determined as stable between the periods May 2016 and August 2017. The reservoir water level increased, reaching about 374 m in August 2017. The reservoir water level dropped by 15 m between May 2016 and August 2017.

The horizontal displacements were detected in upstream direction between the periods May 2016-November 2016, May 2016-May 2017 and May 2016-August 2017. The results showed that the horizontal displacements on the dam crest were caused by the reduction of the reservoir water level. The largest horizontal displacement was found at the object point of 1115 (i.e., 2.97 cm), considering all the horizontal measurements conducted in all periods. The monthly average speed on the object point of 1115 for the May 2016-November 2016, May 2016-May 2017 and May 2016-August 2017 are 3.6 mm, 1.6 mm and 2.0 mm, respectively. It was also observed that the horizontal displacements gradually decreased towards the left and right abutments. Despite this decrease, the horizontal displacements for the object points 1103 and 1139 were found 0.63 cm and 0.68 cm between the periods May 2016 and May 2017, respectively. Although the reservoir water level difference between the periods May 2016 and May 2017 was 10 m greater than that between the periods May 2016 and November 2016, the horizontal displacements showed an increasing trend in upstream direction at all object points, except the 1115 and 1121.

To illustrate the horizontal displacements, the value of the horizontal displacement vector ($d_{horizontal}$) and its direction (α) were computed for each point as below:

$$d_{horizontal} = \sqrt{{d_n}^2 + {d_e}^2}, \alpha = arctan(d_e/d_n) \tag{14}$$

The components of the confidence ellipse, which are the semimajor axes A_i and B_i, and the orientation of the major axis φ_i, are determined for each point as follows:

$$\begin{aligned} A_i &= s_0(2\lambda_{i,1}F)^{1/2} \\ B_i &= s_0(2\lambda_{i,2}F)^{1/2} \end{aligned} \tag{15}$$

$$\varphi_i = \frac{1}{2} arctan \frac{2q_{dnde}}{q_{dndn} - q_{dede}} \tag{16}$$

with

$$\begin{aligned} \lambda_{i,1} &= \frac{1}{2}\left[q_{dndn} + q_{dede} + (\Delta_i)^{1/2}\right] \\ \lambda_{i,2} &= \frac{1}{2}\left[q_{dndn} + q_{dede} - (\Delta_i)^{1/2}\right] \\ \Delta_i &= (q_{dndn} - q_{dede})^2 + 4q_{dnde}^2 \end{aligned} \tag{17}$$

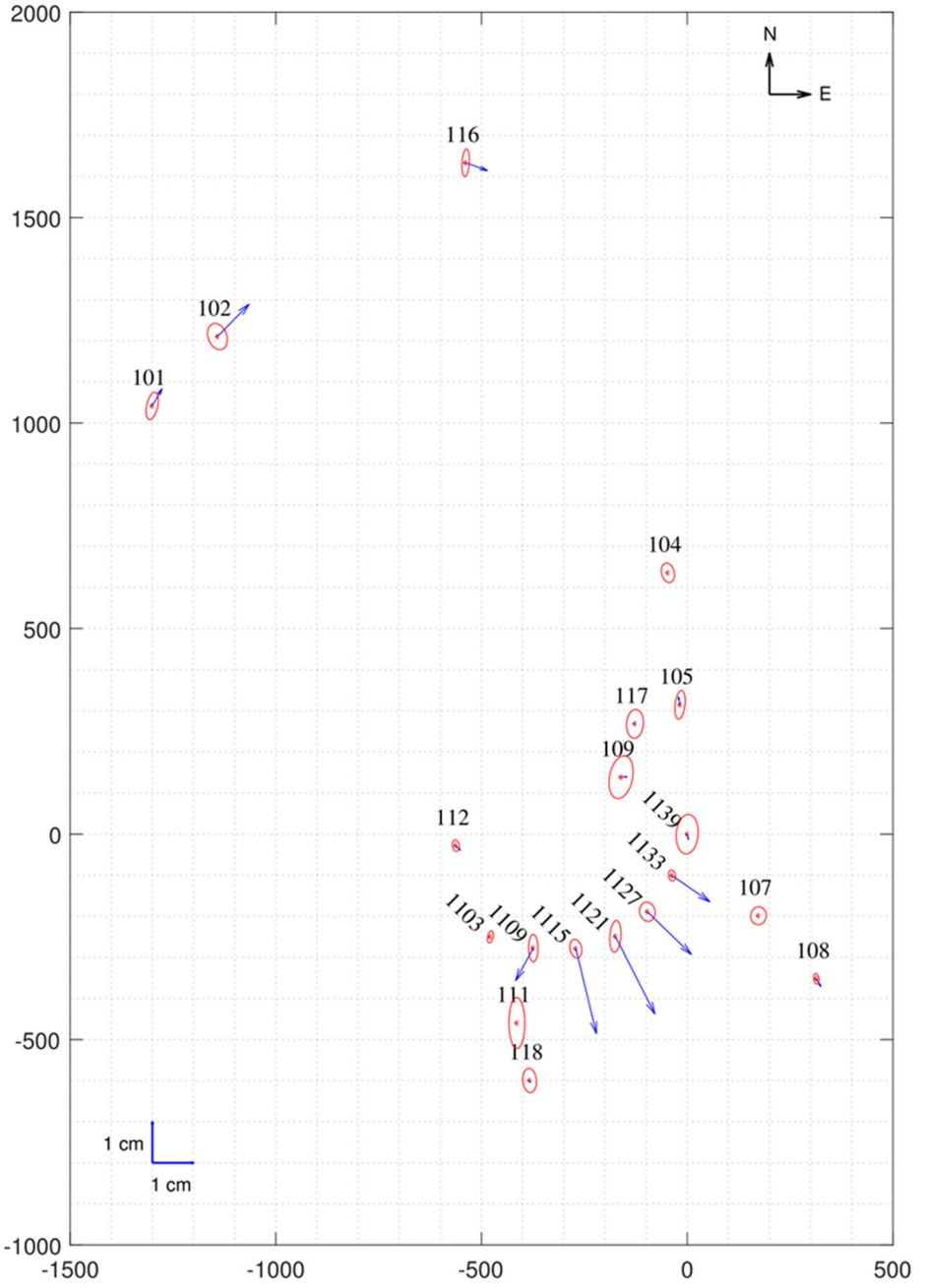

Figure 4. The horizontal displacement vectors for the reference and object points within 95% confidence ellipses between the periods May 2016 and November 2016.

If the horizontal displacement vector lies within the confidence ellipse, the horizontal displacement is considered insignificant. Otherwise, it is considered significant. The horizontal displacements and confidence ellipses were computed and demonstrated in Figures 4–6 for the periods May 2016-November 2016, May 2016-May 2017 and May 2016-August 2017, respectively.

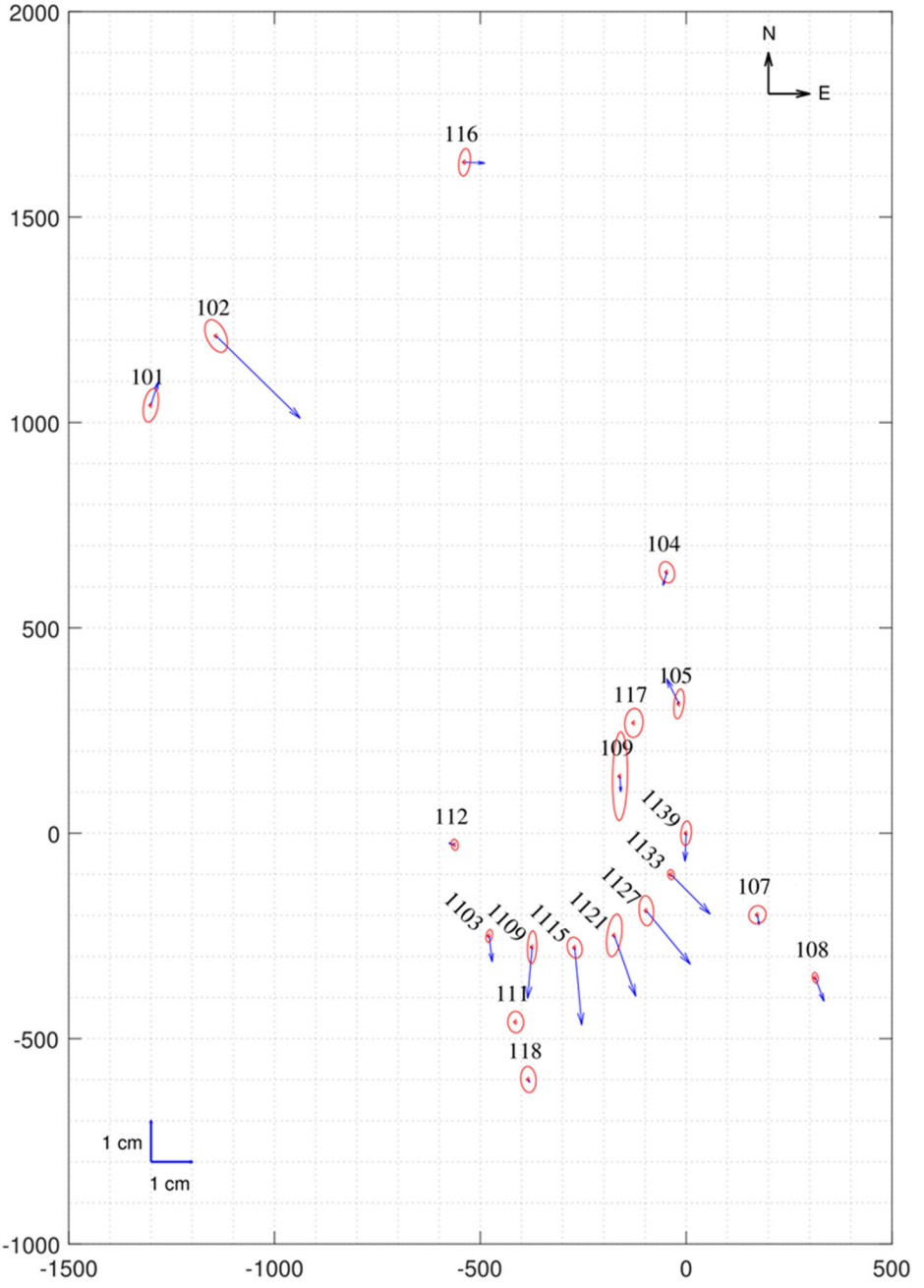

Figure 5. The horizontal displacement vectors for the reference and object points within 95% confidence ellipses between the periods May 2016 and May 2017.

Figure 4 shows that the horizontal displacements at the reference points of 101, 102, 105, 108, 109, 112 and 116, and object points of 1109, 1115, 1121, 1127 and 1133 were insignificant between the periods May 2016 and November 2016. Between the periods May 2016 and May 2017, the horizontal displacements at the reference points of 101, 102, 104, 105, 107, 108, 112 and 116, and at all object points were

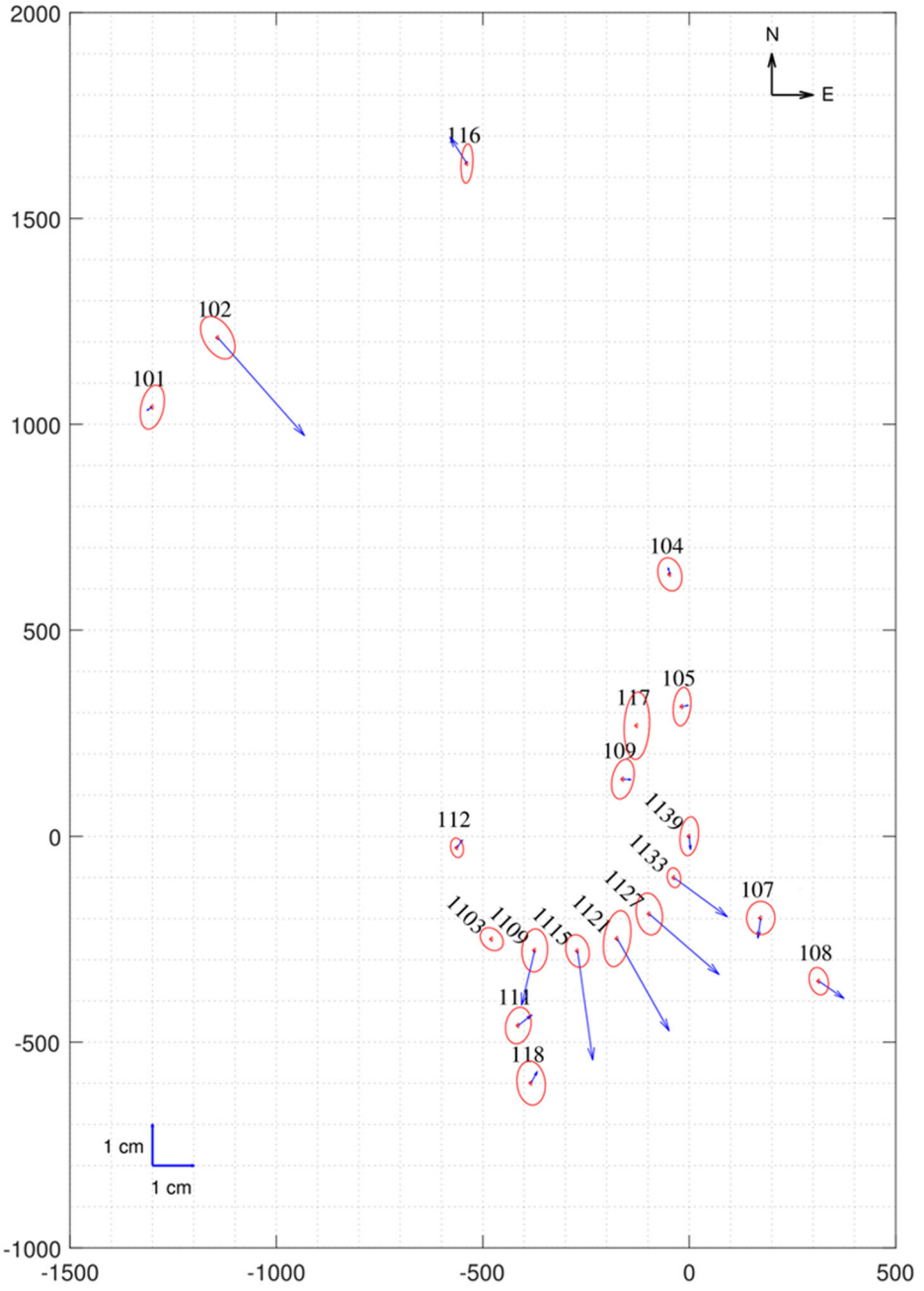

Figure 6. The horizontal displacement vectors for the reference and object points within 95% confidence ellipses between the periods May 2016 and August 2017.

considered insignificant (see Figure 5). The horizontal displacements at the reference points of 102, 107, 108, 112, 116 and 118, and at all the object points except the 1103 were considered insignificant between the periods May 2016 and August 2017 (see Figure 6).

5. Conclusion

In this paper, we investigated the behaviour of the Deriner dam by using the GNSS and high precision leveling observations during the operation phase. The redundancy value, and internal and external reliability values were calculated to evaluate the reliability of the geodetic network. The redundancy values, and internal and external reliability values did not exceed the critical values for all baselines, which shows the robustness of the geodetic network used. The θ^2-criteria was carried out to determine the displacements obtained with the GNSS measurements in three dimensions. Due to the separation capacity of the θ^2-criteria, most of the reference and object points were determined as unstable. As expected, the most significant horizontal and vertical displacements were found in the middle of the dam crest. It was observed that the extent of the displacements decreased towards the end of the dam crest. The results revealed that the horizontal displacements were affected by the reservoir water level. One of the most significant findings emerged from this study is that the GNSS technique can be profitably used to accurately monitor the horizontal displacements of an arch dam. When the vertical displacement values were examined, it was found that these values were higher than expected. Since it has been about 3-4 years after the first filling phase of the dam, vertical displacement values were expected to be either below the cm level or at the mm level. The first filling phase of the dam can be considered as the period in which the displacement is expected to be maximum. The vertical displacements of the dam were examined and reported by the Turkish General Directorate of State Hydraulic Works (DSI) in the first filling phase. (Electrowatt Engineering Ltd and Dolsar Engineering Ltd, 2014). This unpublished report revealed that the maximum amount of vertical displacement was about 2.5 cm as a result of the measurements made at the leveling points that were very close to the piles used in the study. The same report also depicts that displacements are gradually decreasing. From this situation, it can be interpreted that the expected vertical settlement of the dam has slowed down. On the other hand, when the points on the dam crest were compared against each other, it was seen that the movement directions were not consistent with each other. The object points were established on balconies in the dam crest as a pile. The balconies were checked for any cracks or subsidence, or for any deformation of the piles, but none of these were observed. For these reasons, the vertical displacements found in this study can be considered erroneous. The reason for not obtaining sufficient sensitivity in the vertical direction was due to the narrow topography of the valley where the dam was built. As known, narrow valley structure impairs the signal quality between the receiver and satellite. The best way to avoid this is to use a greater (i.e., greater than all the obstacles) cut-off angle. Our experiments revealed that increasing the elevation angle caused the exclusion of many good observations from the GNSS data and that the optimum elevation angle had to be 15°. It can be concluded that this situation affects the precision of vertical positions and may be solved by increasing the observation time in future studies with GNSS. Future research will focus on investigating the behaviour of dams with a kinematic deformation analysis model based on Kalman filtering. In addition to the geodetic deformation analyses, numerical analyses can be conducted and possible displacements can be compared against the geodetic results.

Acknowledgements

The authors would like to thank the Turkish General Directorate of State Hydraulic Works (DSI) and the 26th Regional Directorate Artvin. This paper is a part of Berkant Konakoglu's PhD thesis. This work was also partly supported by the Karadeniz Technical University Scientific Research Projects Coordination Unit with Grant No. 5482. We would also like to express our sincere gratitude to Prof. Dr. Mualla Yalcinkaya from the Department of Geomatics Engineering of Karadeniz Technical University for her support. Finally, our special thanks go to the anonymous reviewers for their constructive comments and suggestions that contributed a lot to the quality of this study.

Disclosure statement

No potential conflict of interest was reported by the authors.

ORCID

Berkant Konakoglu http://orcid.org/0000-0002-8276-587X
Leyla Cakir http://orcid.org/0000-0001-6624-4727
Volkan Yilmaz http://orcid.org/0000-0003-0685-8369

References

Acar M, Ozludemir MT, Erol S, Celik RN, Ayan T. 2008. Kinematic landslide monitoring with Kalman filtering. Nat Hazards Earth Syst Sci. 8(2):213–221.

Acosta L, de Lacy M, Ramos M, Cano J, Herrera A, Avilés M, Gil A. 2018. Displacements study of an earth fill dam based on high precision geodetic monitoring and numerical modeling. Sensors. 18(5):1369.

Baarda W. 1968. A testing procedure for use in geodetic networks. Netherlands Geodetic Commission. 2(5).

Barzaghi R, Cazzaniga NE, De Gaetani CI, Pinto L, Tornatore V. 2018. Estimating and Comparing Dam Deformation Using Classical and GNSS Techniques. Sensors. 18(3):756.

Bayrak T. 2007. Modelling the relationship between water level and vertical displacements on the Yamula Dam. Nat Hazards Earth Syst Sci. 7(2):289–297.

Bayrak T. 2008. Verifying pressure of water on dams, a case study. Sensors. 8(9):5376–5385.

Caspary WF. 1988. Concepts of network and deformation analysis. Monograph 11, 2nd corrected impression. Kensington: School of Surveying, The University of New South Wales. p. 183.

Cooper M. 1987. Control surveys in civil engineering. London: Collins.

De Sortis A, Paoliani P. 2007. Statistical analysis and structural identification in concrete dam monitoring. Eng Struct. 29(1):110–120.

Di Pasquale A, Nico G, Pitullo A, Prezioso G. 2018. Monitoring strategies of earth dams by ground-based radar interferometry: how to extract useful information for seismic risk assessment. Sensors. 18(1):244.

Ehiorobo JO, Irughe-Ehigiator R. 2011. Monitoring for horizontal movement in an earth dam using differential GPS. J Emerg Trends Eng Appl Sci. 2(6):908–913.

Electrowatt Engineering Ltd and Dolsar Engineering Ltd. 2014. Deriner Dam and hydroelectric power plant geodetic dam monitoring I8 readings after completion of impounding. Technical Report. Ankara: Electrowatt Engineering Ltd. and Zurich. Dolsar Engineering Ltd.

Erol S, Erol B, Ayan T. 2005. Analyzing the deformations of a bridge using GPS and levelling data. Proceeding of Geodetic Deformation Monitoring: From Geophysical to Engineering Roles; Mar 17–19; Jaén, Spain. p. 244–253.

Gikas V, Sakellariou M. 2008. Settlement analysis of the Mornos earth dam (Greece): Evidence from numerical modeling and geodetic monitoring. Eng Struct. 30(11):3074–3081.
Guler G, Kilic H, Hosbas G, Ozaydın K. 2006. Evaluation of the movements of the dam embankments by means of geodetic and geotechnical methods. J Surv Eng. 132(1):31–39.
Hastaoğlu KÖ. 2013. Investigation of the groundwater effect on slow-motion landslides by using dynamic Kalman filtering method with GPS: Koyulhisar town center. Turk J Earth Sci. 22(6):1033–1046.
Huber PJ. 1981. Robust statistics. New York (NY): Wiley.
Kalkan Y. 2014. Geodetic deformation monitoring of Ataturk Dam in Turkey. Arab J Geosci. 7(1):397–405.
Kanik M, Ersoy H. 2019. Evaluation of the engineering geological investigation of the Ayvali dam site (NE Turkey). Arab J Geosci. 12(3):89.
Kayikci ET, Yalcinkaya M. 2015. Determination of horizontal movements by static deformation models: a case study on the mining area. Exp Tech. 39(6):70–81.
Koch KR. 1985. Ein statistisches auswerteverfahren für deformationsmessungen. Allg Vermessung-Nachr. 92(3):97–108.
Kulkarni MN, Radhakrishnan N, Rai D. 2006. Global positioning system in disaster monitoring of Koyna dam, Western Maharashtra. Surv Rev. 38(301):629–636.
Küreç P, Konak H. 2014. A priori sensitivity analysis for densification GPS networks and their capacities of crustal deformation monitoring: a real GPS network application. Nat Hazards Earth Syst Sci. 14(5):1299–1308.
Manake A, Kulkarni MN. 2002. Study of the deformation of Koyna dam using the Global Positioning System. Surv Rev. 36(285):497–507.
Mascolo L, Nico G, Di Pasquale A, Pitullo A. 2014. Use of advanced SAR monitoring techniques for the assessment of the behaviour of old embankment dams. Proc SPIE 9245, Earth Resources and Environmental Remote Sensing/GIS Applications V, 9245:92450N.
Niemeier W. 1985. Deformations analyse. In: H. Pelzer, editor. Geodaetische Netze in Landes – und Ingenieurvermessung II. Stuttgart: Konrad Wittwer. p. 559–623.
Ozener H, Dogru A, Acar M. 2013. Determination of the displacements along the Tuzla fault (Aegean region-Turkey): Preliminary results from GPS and precise leveling techniques. J Geodyn. 67:13–20.
Pelzer H. 1985. Geodatische netze in landes- und ingenieurvermessung II. Stuttgart: Wittwer Verlag.
Pelzer H. 1971. Zur analyse geodätischer deformationsmessungen. München (Germany): Deutsche Geodätische Kommission, C-164.
Pytharouli SI, Stiros SC. 2005. Ladon dam (Greece) deformation and reservoir level fluctuations: evidence for a causative relationship from the spectral analysis of a geodetic monitoring record. Eng Struct. 27(3):361–370.
Sabuncu A, Ozener H. 2014. Monitoring vertical displacements by precise levelling: a case study along the Tuzla Fault, Izmir, Turkey. Geomat Nat Haz Risk. 5(4):320–333.
Saidi S, Houimli H, Zid J. 2017. Geodetic and GIS tools for dam safety: case of Sidi Salem dam (northern Tunisia). Arab J Geosci. 10(22):505.
Talich M. 2016. The deformation monitoring of dams by the ground-based InSAR technique-case study of concrete hydropower dam Orlík. Int J Adv Agric Environ Eng. 3(1):192–197.
Tarchi D, Rudolf H, Luzi G, Chiarantini L, Coppo P, Sieber A J. 1999. SAR interferometry for structural changes detection: A demonstration test on a dam. In: IEEE 1999 International Geoscience and Remote Sensing Symposium. IGARSS'99. Vol. 3. p. 1522–1524.
Taşçi L. 2008. Dam deformation measurements with GPS. Geod Cartogr. 34(4):116–121.
Teunissen PJ. 1985. Zero order design: Generalized inverses, adjustments, the datum problem and S-transformations. In: Grafarend E. W., Sanso F, editors. Optimization and design of geodetic networks. Berlin, Heidelberg, New York: Springer; p. 11–55.
Tiryakioglu I, Yigit CO, Ozkaymak C, Baybura T, Yilmaz M, Ugur MA, Yalcin M, Poyraz F, Sözbilir H, Gulal VE. 2019. Active surface deformations detected by precise levelling surveys in the Afyon-Akşehir Graben, Western Anatolia, Turkey. Geofizika. 36(1):33–52.

Xi R, Zhou X, Jiang W, Chen Q. 2018. Simultaneous estimation of dam displacements and reservoir level variation from GPS measurements. Measurement. 122:247–256.

Xiao R, Shi H, He X, Li Z, Jia D, Yang Z. 2019. Deformation monitoring of reservoir dams using GNSS: an application to South-to-North Water Diversion Project, China. IEEE Access. 7:54981–54992.

Yalçinkaya M, Bayrak T. 2005. Comparison of static, kinematic and dynamic geodetic deformation models for Kutlugün landslide in northeastern Turkey. Nat Hazards. 34(1):91–110.

Yalçınkaya M, Teke K. 2006. Optimization of GPS Networks with respect to the accuracy and reliability criteria. Proceeding of the XXIII International Fig Congress; Oct 8–13; Münih, Germany.

Yavaşoğlu HH, Kalkan Y, Tiryakioğlu İ, Yigit CO, Özbey V, Alkan MN, Bilgi S, Alkan RM. 2018. Monitoring the deformation and strain analysis on the Ataturk Dam, Turkey. Geomat Nat Haz Risk. 9(1):94–107.

Yigit CO. 2016. Experimental assessment of post-processed kinematic precise point positioning method for structural health monitoring. Geomat Nat Haz Risk. 7(1):360–383.

Yigit CO, Alcay S, Ceylan A. 2016. Displacement response of a concrete arch dam to seasonal temperature fluctuations and reservoir level rise during the first filling period: evidence from geodetic data. Geomat Nat Haz Risk. 7(4):1489–1505.

Zeybek M, Şanlıoğlu İ, Özdemir A. 2015. Monitoring landslides with geophysical and geodetic observations. Environ Earth Sci. 74(7):6247–6263.